Ch. 3: Experimental

****

This chapter mainly deals with the description of the preparation of blend polymer electrolyte specimens and cathodes followed by the detailed discussion on various experimental techniques that are used to characterize the as prepared materials.

****

3.1 Sample Preparation

The present work deals with the preparation of the blend polymer electrolytes and cathode materials which are later considered in the battery applications. Details of the preparation of the as mentioned specimens are as follows.

3.1.1 Preparation of Blend Polymer Electrolytes

Commercially available Analytical Reagent (AR) grade starting chemicals used to prepare blend polymer electrolytes in the present work are tabulated in Table 3.1.

Table 3.1 Starting materials considered for the preparation of blend polymer electrolytes

Sr. No.	*Starting Materials*	*Molecular Weight (M.W.)*	*Company*
1	Polyvinyl Alcohol (PVA)	1,15,000	Lobachemie
2	Polyethylene Oxide (PEO)	1,000,000	Alfa Aesar
3	Silver Nitrate ($AgNO_3$)	169.89	Sarabhai Chemicals
4	Lithium Trifluoromethane-Sulfonate ($LiCF_3SO_3$)	F.W. 156.01	Sigma Aldrich
5	Polyethylene Glycol (PEG)	3,500 - 4,000	Lobachemie
6	Ethylene Carbonate (EC)	88.06	Sigma Aldrich
7	Aluminium Oxide (Al_2O_3)	101,96 g/mol Particle size < 50 nm	Sigma Aldrich
8	Deionized Water	--------	--------

In the preparation of these blend electrolytes, PVA and PEO have served as host polymers, $AgNO_3$ and $LiCF_3SO_3$ as dopant salts, PEG and EC as plasticizers, Al_2O_3 as nano-filler and deionized water as solvent. These electrolytes are synthesized using *'Solution (Solvent) Cast Technique'*, also termed as *'Solution Casting'* [1-5].

❖ ***General Theory of Solution Cast Technique***

Solution cast technique is employed in the preparation of the present blend polymer electrolytes owing to its advantageous properties such as high simplicity, low mould costs, ability to solidify large parts with thin as well as thick cross-sections, energetic and economical cheapness, capability to be conducted easily at ordinary temperatures and

pressures, easy producibility of polymeric films with desired shapes and sizes as well as uniform transparency and distribution hence, yielding good surface finish of the obtained product [6]. Generally, in this technique, the selected materials (polymers and additives) are weighed in the desired proportion using analytical balance and mixed stoichiometrically in the common solvent at suitable temperatures (either room temperatures or at temperatures above room temperature as per requirement). These materials are then mixed one by one in the solvent. This solution is then stirred for a few hours till it appears homogeneous. The hence, obtained solution is then poured in a teflon petridish and allowed to dry at temperatures ≥ room temperatures at which the solvent can evaporate. During the evaporation process of the solvent, the complexation of polymers and salts is said to occur if there is a strong interaction between polymers and ions of the salt. After the complete evaporation of the solvent, the dried polymer films are peeled off from the petridish and preserved in vacuum desiccator to prevent from moisture.

❖ ***Synthesis of Blend Polymer Electrolyte Series for the Present Work***

Mainly 5 blend polymer electrolyte series are prepared for the present work. The schematic description of these series is as provided.

1) ***PPAP Series:*** $[PVA_{(100-x)} : PEO_{(x)}] - 5$ wt% $AgNO_3 - 10$ wt% PEG
where, x = 10 % to 50 % in the steps of 10

2) ***PPAPA Series:*** $[PVA_{(50)} : PEO_{(50)}] - 5$ wt% $AgNO_3 - 10$ wt% PEG – x wt% Al_2O_3
where, x = 2 wt% to 10 wt% in the steps of 2

3) ***PPLE Series:*** $[PVA_{(50)} : PEO_{(50)}] - 5$ wt% $LiCF_3SO_3$ – x wt% EC
where, x = 2 wt% to 10 wt% in the steps of 2

4) ***PPEL Series:*** $[PVA_{(50)} : PEO_{(50)}] - 6$ wt% EC – x wt% $LiCF_3SO_3$
where, x = 3 wt% to 11 wt% in the steps of 2

5) ***PPELA Series:*** $[PVA_{(50)} : PEO_{(50)}] - 6$ wt% EC – 9 wt% $LiCF_3SO_3$ – x wt% Al_2O_3
where, x = 2 wt% to 10 wt% in the steps of 2

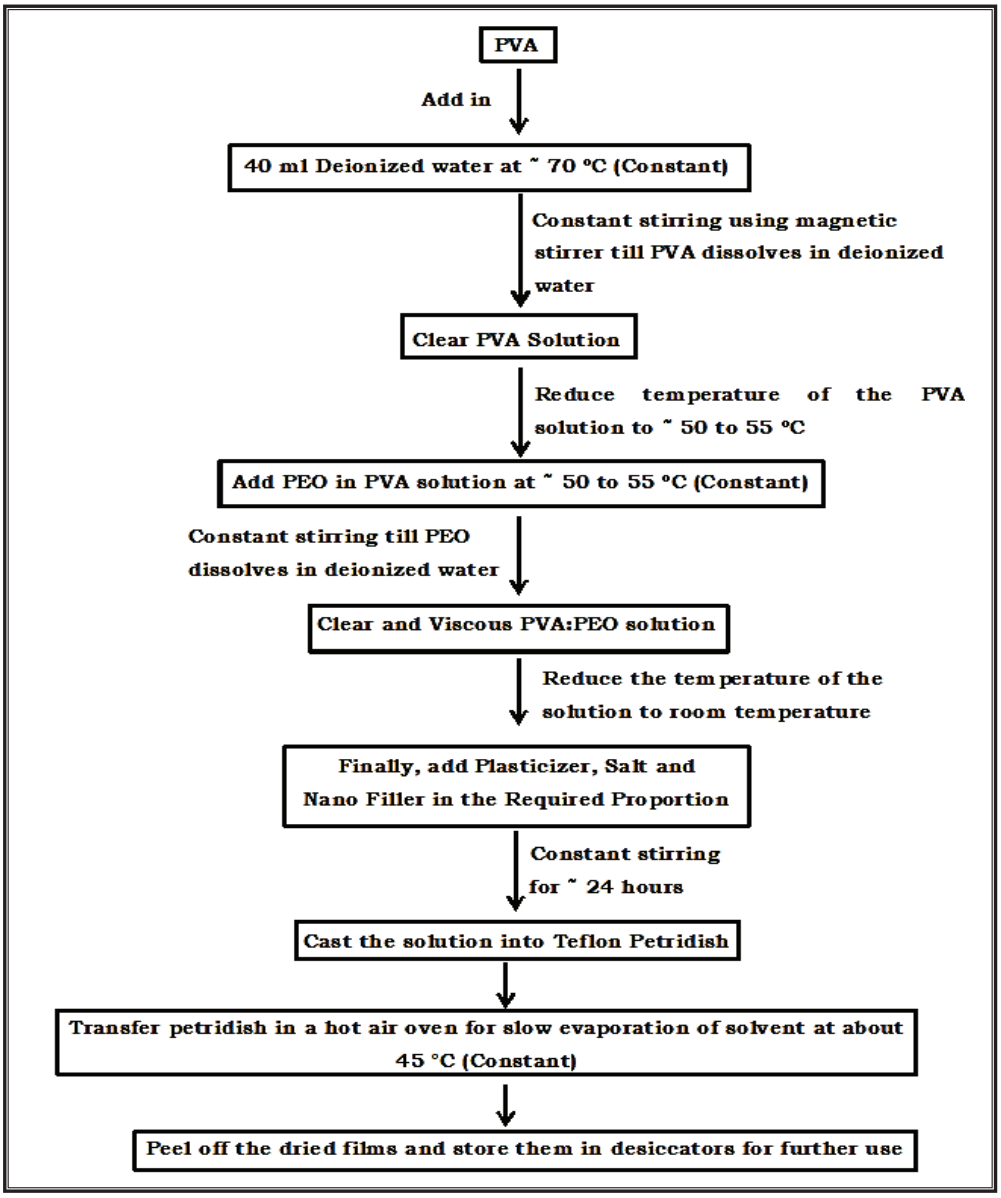

Blend polymer electrolyte specimen with $AgNO_3$ salt

Blend polymer electrolyte specimen with $LiCF_3SO_3$ salt

Fig. 3.1 Flow chart describing the synthesis of blend polymer electrolyte specimens

Fig. 3.2 (a) Analytical balance

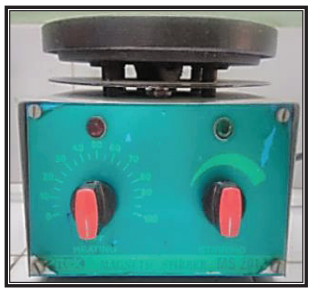

Fig. 3.2 (b) Magnetic stirrer

The ***'Solution Cast'*** procedure of synthesising the blend polymer electrolyte specimens of the above mentioned series is commonly described in the form of a flow chart as shown in Fig. 3.1. The constituents and their amounts (expressed as percentage (%) or weight percentage *(wt%)*), in the preparation of these blend specimens, are chosen with respect to the series considered where, the respective constituents are firstly weighed using *'Analytical Balance'* as shown in Fig. 3.2 (a) and then added proportionately in deionized water taken as a common solvent. This solution is later stirred using the *'Magnetic Stirrer'* as shown in the Fig. 3.2 (b) for suitable time of 24 hours. Thickness of the thus, prepared blend specimens for all the considered series ranged from 0.005 cm to 0.015 cm.

3.1.2 Preparation of Cathodes

Present work includes the preparation of silver oxide (Ag_2O) and lithium manganese oxide ($LiMn_2O_4$) cathodes. The basic constituent used in the preparation of Ag_2O cathode is pure Ag_2O chemical (Molecular Weight (M.W.) = 231.74, Sisco Research Laboratories (SRL)) whereas; $LiMn_2O_4$ cathode is synthesised using Extrapure AR Grade lithium carbonate (Li_2CO_3) (Molecular Weight (M.W.) = 73.89, Sisco Research Laboratories (SRL)) and pure manganese carbonate ($MnCO_3$) (Molecular Weight (M.W.) = 114.95, Sisco Research Laboratories (SRL)). In the synthesis of both Ag_2O and $LiMn_2O_4$ mixtures,

polyvinyl alcohol (PVA) is used as common binder which is prepared by using the following steps.

- ❖ Small amount of PVA polymer is added in the freshly prepared deionized water (solvent).
- ❖ This mixture is then stirred continuously using a magnetic stirrer at a constant temperature of 70 ºC to 80 ºC for about 2-3 hours till the solution appears viscous, clear and homogeneous.
- ❖ This PVA solution is then gradually cooled down to room temperature and stored in a desiccator for its further use as 'binder' in the preparation of Ag_2O and $LiMn_2O_4$ cathodes.

The major purpose of selecting PVA as binder in the preparation of these cathodes is its *'Hydroxyl Groups'* which not only facilitate the transport of hydroxyl ions to the electrode surface but also aid mechanical stability to thus, prepared Ag_2O and $LiMn_2O_4$ cathodes [7].

♣ ***Preparation of Ag_2O Cathode***

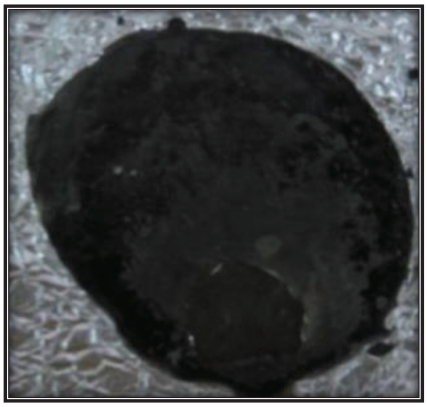

Fig. 3.3 Ag_2O cathode

For preparing the silver oxide (Ag_2O) cathode, as depicted in Fig. 3.3, firstly, the required amount of Ag_2O powder is taken into mortar pestle and ground gently for about half an hour to obtain a 'fine' Ag_2O powder. This finely ground Ag_2O powder is then transferred to glass petridish into which a few drops of PVA binder is added. This Ag_2O powder is then mixed gently with the added PVA binder to leave a syrupy mixture of Ag_2O-PVA into the

petridish. This mixture is then poured on an aluminium foil followed by its very thin layered even coating on the foil of nearly 0.020 cm. This foil is then transferred into a hot air oven for drying at a constant temperature of about 70 ºC to 80 ºC for the complete evaporation of the solvent. The dried film (foil) of Ag_2O-PVA mixture is then stored in vacuum desiccator and used later as 'cathode' in the 'Ag^+ primary polymer battery' assembly.

♣ ***Preparation of $LiMn_2O_4$ Cathode***

In the preparation of $LiMn_2O_4$ cathode as shown in Fig. 3.4 (a) firstly, Li_2CO_3 and $MnCO_3$ chemicals are weighed as per pre-determined molar ratio of Li:Mn = 1:2. These chemicals are then taken into mortar pestle and ground gently for about 30 min to obtain a perfect and fine mixture which is then transferred into a porcelain crucible. The crucible is then placed into a muffle furnace as depicted in Fig. 3.4 (b). The temperature of this furnace is raised gradually to 400 ºC and kept constant for about an hour so as to remove the moisture and unwanted gases from the mixture. After an hour, the furnace is switched off and the mixture therein is allowed to cool down slowly to room temperature.

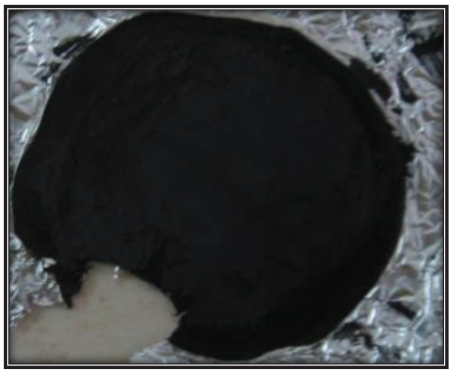

Fig. 3.4 (a) $LiMn_2O_4$ cathode

Fig. 3.4 (b) Muffle furnace

After cooling, this mixture is then again taken into mortar pestle, crushed gently for about 30 min, transferred into a new crucible and kept back into muffle furnace. But at this stage, the temperature of the furnace to reheat the mixture is raised to 700 ºC and kept

constant for an hour. After an hour, the furnace is switched off and the mixture is allowed to cool down gently to room temperature in the furnace itself. This hence, obtained mixture of $LiMn_2O_4$ powder is taken into a glass petridish wherein, a few drops of PVA binder is added and mixed gently with it so as to yield a fine paste of $LiMn_2O_4$-PVA. A thin layer of nearly 0.015 cm of this as obtained paste is then coated on an aluminium foil. This foil is then transferred into a hot air oven for drying at a constant temperature of about 70 ºC to 80 ºC till the solvent evaporates completely from it. The completely dried film of $LiMn_2O_4$-PVA mixture is then stored into a vacuum desiccator and later used as 'cathode' in the 'Li^+ primary polymer battery assembly'. This method of preparation of $LiMn_2O_4$ powder, considered in the present research work is termed as *'Solid State Reaction'* technique [8,9].

In the making of both these Ag_2O as well as $LiMn_2O_4$ cathodes, aluminium metal (foil) is used as current collector due to its low price, high purity and appreciable electrical conductivity [10].

3.2 Experimental Techniques

Characterization studies of the hence, prepared blend polymer electrolyte specimens and cathodes are done by various experimental techniques which include X-ray diffraction, differential scanning calorimetry, Fourier transform infrared spectroscopy, scanning electron microscopy and ionic transport number measurement.

3.2.1 X-Ray Diffraction

'X-ray diffraction (XRD)' is one of the fastest, convenient and versatile non-destructive methods used for gross qualitative and quantitative characterization of materials in the field of solid state chemistry and materials science which determines their physical characteristics [11]. The instrumental setup which carries out such characterization studies is known as *'X-Ray Diffractometer'*, the block diagram of which is as shown in Fig. 3.5.

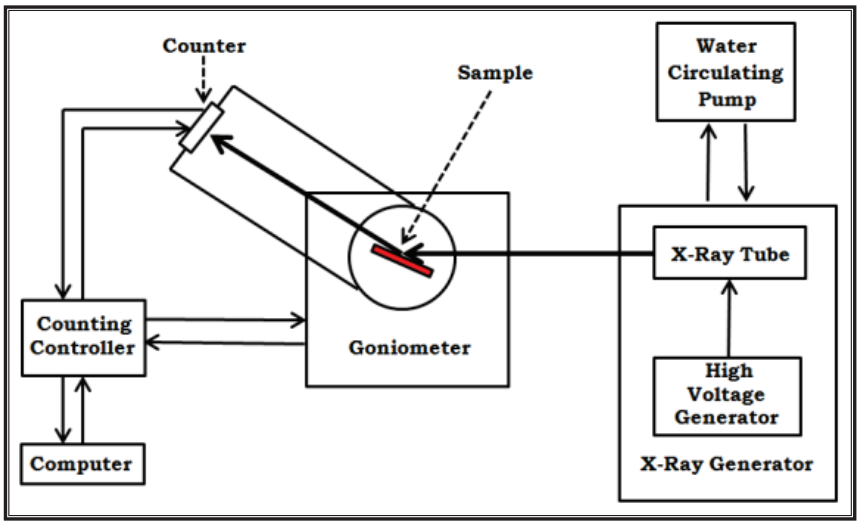

Fig. 3.5 Block diagram of X-ray diffractometer

This instrument consists of a source of X-rays which can be either cathode ray tube (CRT) or X-ray tube. This source consists of a tungsten filament which when heated electrically by applying current, produces electrons. The electron beam of the hence, produced electrons is then accelerated towards the anode/target by applying the high voltage of about 30 kV. This accelerated electron beam when allowed to strike at the stationary or rotating metallic (Cr, Fe, Mo, Cu) target produces X-ray photons, having the energy characteristics same as that of the target material. But in this process, only a small fraction of energy of the incident electron beam is converted to X-rays whereas; the rest is transformed into heat. But the hence, produced heat can easily melt down the anode. To prevent so, it is highly essential to continuously cool down the anode with chilled water which is provided by the water circulating pump.

These hence produced X-rays, also known as *'Braking Radiations'* or *'Bremsstrahlung Radiations'* having a short wavelength from a few Å to 0.1 Å and 1 keV to 120 keV, are used to probe structural arrangements of atoms and molecules in a variety of materials viz. polymer electrolytes. These resulting X-rays comprising of several wavelengths pass through 'Fe' or 'Zn' filter, which are usually as foils or crystal monochromators. The filter eliminates the

unwanted radiations of undesired wavelengths and transmits only monochromatic X-rays of desired wavelengths. The coherent X-ray photons are finally directed onto the sample under test [9,12]. The atoms (or ions) of the same plane or from neighbouring planes of the sample act as secondary point sources and reflect the incident X-ray beam thus, leading to *'Interference'*. In case X-rays impinging sample satisfies Bragg's equation given as Eq. 3.1, constructive interference occurs wherein; the reflected X-ray beams are 'in phase' as also seen from Fig. 3.6 [6,9,13-16].

$$n\lambda = 2d \sin\theta \qquad \ldots\ldots\ldots\ldots\ldots (3.1)$$

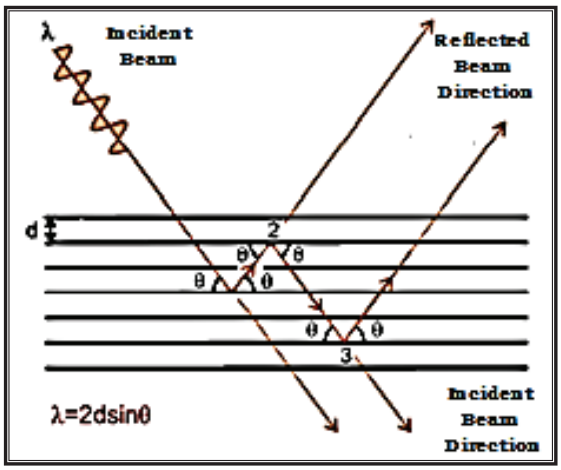

Fig. 3.6 Schematic diagram of reflection of x-rays by a crystalline sample

On the contrary, if Bragg's law is not satisfied, the reflected X-ray beams are 'out of phase', leading to the destructive inference. The intensity and direction of the hence, reflected X-rays are detected by the detector and finally, processed and counted by scanning the sample through the range of '2θ' angles either electronically or by using microprocessor. But in the entire process, the motion of the detector depends upon two major geometries available in the X-ray diffractometers.

θ-2θ Geometry: The X-ray source is stationary. Sample moves by an angle 'θ' and simultaneously, detector moves by angle of '2θ' with respect to X-ray source.

θ-θ Geometry: The sample is stationary. X-ray source along with the detector rotate simultaneously by an angle 'θ', with respect to the sample, but in clockwise and anticlockwise directions, respectively.

These rotations are led by *'Goniometer'* which is the central part of diffractometer. But in the entire process, the efficiency of a detector to collect X-ray photon and to convert it into a measureable signal is its important characteristic. The final output in the form of *'X-Ray Diffraction (XRD) spectrum'* can be obtained via printer or computer monitor and can be interpreted mathematically. In this XRD spectrum the X-axis represents '2θ' angle whereas; the Y-axis refers to the X-ray counts or intensity of X-rays. The relative intensity is recorded by the ratio of the peak under consideration to the intensity of the most intense peak [17-20].

The constructive interference leads to sharp diffraction peaks referring to crystalline phase whereas; the destructive interference shows less intense peaks and/or humps corresponding to the amorphous phase. In this way, the analysis of the XRD spectrum gives an idea regarding the crystalline and/or amorphous phases present/formed in a material. A single crystalline solid sample possessing perfect ordering of crystallites therein is investigated using *'Single Crystal X-Ray Diffraction'* method. However, the polycrystalline polymers are examined using *'Powder X-Ray Diffraction'* method.

♣ **Present Study**

The nature of the phase (crystalline/amorphous) present/formed in the as prepared PVA-PEO blend specimens as well as cathode materials is investigated by recording and analysing their respective XRD patterns at room temperature using 'X-Ray Powder Diffractometry'. The XRD measurements of pure PVA and PEO polymers along with those of the blend specimens of PPAP and PPAPA series are carried out using *'Shimadzu Diffractometer'* XRD instrument as depicted in Fig. 3.7 (a), at a scan rate of 2°/min and those of the blend specimens of PPLE, PPEL and PPELA series as well as of $LiMn_2O_4$ cathode are done by

using *'Bruker Powder XRD Model D2 Phaser'* XRD instrument as shown in Fig. 3.7 (b), where scanning time is kept as 0.1 sec. Measurements are taken in '2θ' range of 10° to 70°.

Fig. 3.7 (a) Shimadzu Diffractometer

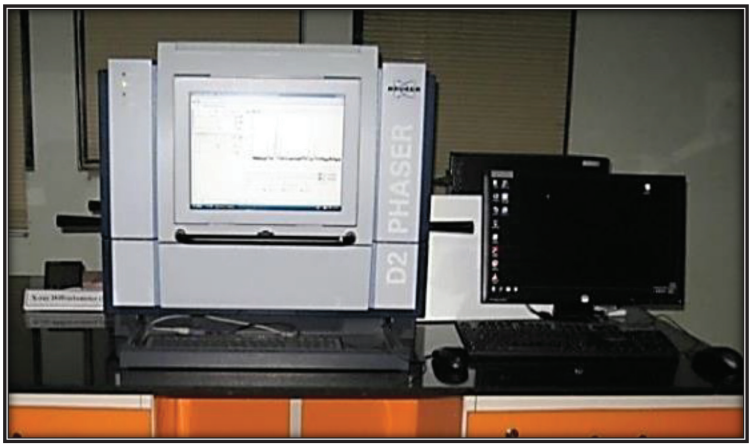

Fig. 3.7 (b) Bruker Powder XRD Model D2 Phaser

3.2.2 Differential Scanning Calorimetry

One of the several techniques to carry out thermal analysis is *'Differential Scanning Calorimetry (DSC)'* introduced by **Watson et al.** [1] in 1964. This technique measures the heat capacity or heat flow as a function of temperature, associated with the thermal transitions taking place in the sample viz. polymeric sample under consideration [21-26]. This thermal analysis technique is based on the relationship between properties such as heat of reaction, mass or volume of the system and temperature. Schematic diagram of such a *'Differential*

Scanning Calorimeter' unit is as shown in Fig. 3.8, which consists of a sample pan and a reference pan.

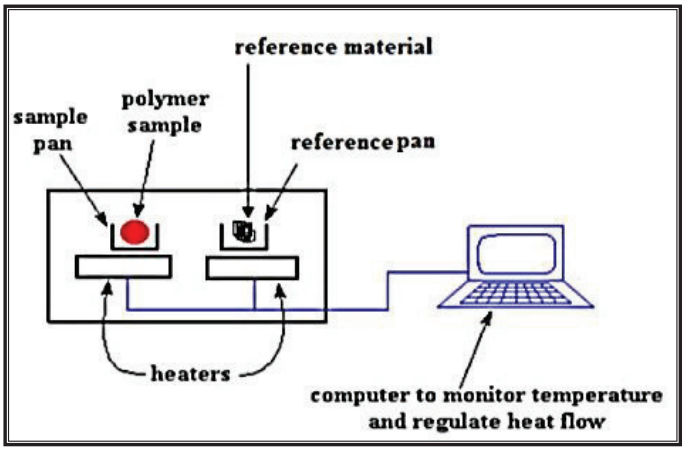

Fig. 3.8 Schematic diagram of differential scanning calorimeter unit

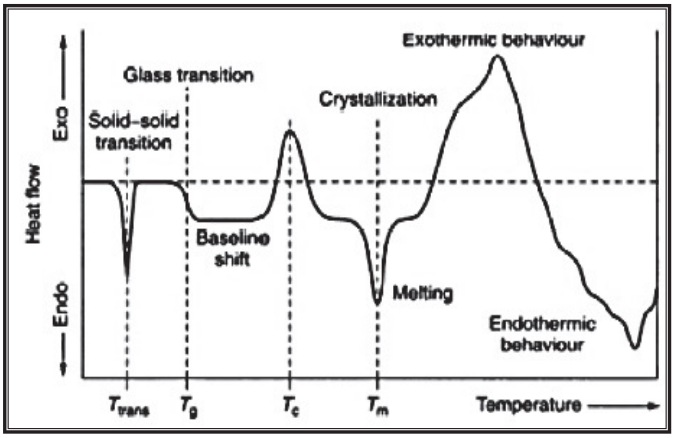

Fig. 3.9 DSC thermogram

Both these pans are made up of metals like aluminium, gold, graphite, platinum or copper to prevent their reactions with the sample. In the sample pan, the sample of nearly 0.5 mg. to 10 mg. is encapsulated (sealed) whereas; the reference pan either contains inert materials or kept empty. These pans are then placed on the raised platforms formed in a constantan disc or heater made up of metal or constantan alloy which act as a primary means of transfer of heat to and from the reference and sample. Both, the sample as well as reference in the respective pans are heated at a specific rate of ~ 10 °C/min or 20 °C/min by turning on the individual heaters. This differential heat flow required for raising the temperature of the

sample and reference, as the heat transfers through the constantan disc, is measured as a function of temperature by the thermocouples that are formed by the junction of constantan disc and chromel wafers covering the underside of the platforms.

The basic working principle of this method is that the temperatures of the sample as well as reference should be maintained to be nearly equal. To fulfil this requirement, extra heat may need to be supplied to either the sample or to the reference [9]. Generally, during the heating process, the sample may either absorb heat or release it leading to the respective endothermic and exothermic processes. Both these processes lead to certain physical transitions termed as *'Phase Transitions'* in the sample. Such exothermic and endothermic heat flows can be measured by differential scanning calorimeter and analysed graphically with respect to temperature from the DSC thermogram as shown in the Fig. 3.9 [27,28]. Various thermal parameters based on these phase transitions and thermal phenomena are explained as follows.

Glass Transition Temperature (T_g): Heat capacity of a polymeric sample changes at glass transition temperature (T_g). However, as no latent heat is either absorbed or released by the sample at this temperature, any peak is rarely observed in the DSC thermogram at 'T_g'. Hence, glass transition temperature is called as *'2nd order phase transition'*. As seen from the DSC thermogram, only a change in flat or horizontal baseline is detected at 'T_g'. However, a peak at 'T_g' can be rarely observed.

Crystallization Temperature (T_c): As crystallization process occurring at crystallization transition temperature 'T_c' is an exothermic process, an exothermic peak is observed at 'T_c' as seen from the DSC thermogram. This process of crystallization transition is termed as *'1st order phase transition'* as it involves latent heat that is given off in the exothermic process.

Melting Temperature (T_m): When a polymeric sample absorbs heat, the crystals present therein melt. As this phenomenon of melting is an endothermic process involving absorption

of latent heat, it is known as *'1st order phase transition'*. The endothermic peak corresponding to this phenomenon occurs at melting temperature 'T_m' as seen from the DSC thermogram.

Degree of Crystallinity (X_c): Area under the melting peak of a particular polymeric sample provides the melting enthalpy of the melting transition which further aids in calculating its degree of crystallinity 'X_c' which can be defined as the *'ratio of melting enthalpy 'ΔH_m'(heat of fusion) of the sample to the melting enthalpy 'ΔH_m^0'(equilibrium heat of fusion) of pure crystalline phase of the sample'* and it is mathematically expressed as [29]:

$$X_c = \frac{\Delta H_m}{\Delta H_m^0} \times 100\% \qquad \ldots\ldots\ldots\ldots\ldots (3.2)$$

♣ ***Present Study***

Fig. 3.10 (a) Crimpier

Fig. 3.10 (b) SII EXSTAR 6000

For the DSC measurements in the present work, thin pieces of the polymer films of about 1-2 mg are taken into the respective sample pans made up of aluminium which are then sealed using *'Crimpier'* as shown in Fig. 3.10 (a). These pans are then placed on the raised platforms of the differential scanning calorimeter to carry out their DSC measurements. The DSC measurements of pure PVA, pure PEO and blend specimens of all the series (except of PPELA series) are carried out using the *'SII EXSTAR 6000'* DSC instrument as shown in the

Fig. 3.10 (b) at a heating rate of 20 °C/min and in the temperature range of 30 °C to 75 °C, except for the pure PVA polymer whose DSC scan is depicted from 30 °C to 230 °C.

.

Fig. 3.10 (c) DSC822^e Mettler Toledo

The measurements of the specimens of PPELA series are carried out using the *'DSC822^e Mettler Toledo'* DSC instrument as depicted in Fig. 3.10 (c), in the temperature range of 30 °C to 75 °C where the heating rate is kept as 10 °C/min. All these measurements are carried out in the nitrogen (N_2) atmosphere. Lastly, the melting temperature (T_m) and degree of crystallinity (X_c) of the blend specimens under test are determined.

3.2.3 Fourier Transform Infrared Spectroscopy

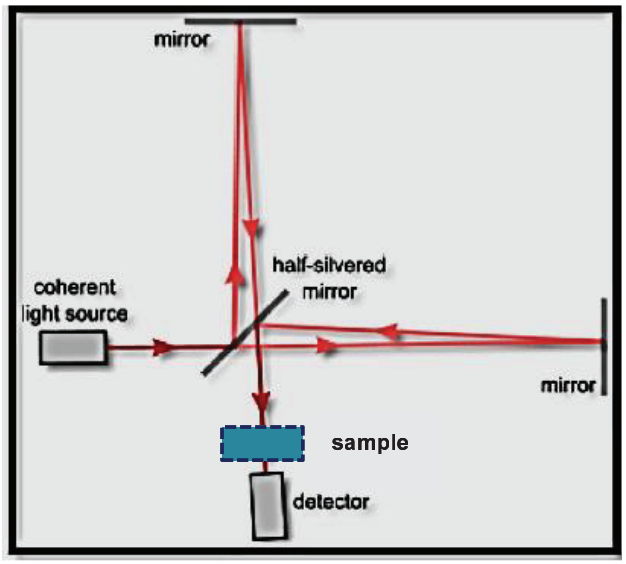

Fig. 3.11 (a) Optical diagram of FT-IR spectrometer with sample

'Fourier Transform Infrared (FT-IR) Spectroscopy' is one of the fastest, versatile and inexpensive techniques to characterize the surface as well as bulk of a material viz. polymer electrolyte. Here, *'Spectroscopy'* is conventionally defined as a 'science of interaction between the matter and infrared radiation' wherein; when infrared (IR) radiations interact with the matter, the radiation only triggers vibrational and/or rotational excitation and not the electronic excitation. In this method, IR radiations produced in the mid-frequency region by a coherent source travel to the beam splitter (half silvered mirror) as shown in Fig. 3.11 (a) and split into two equal halves of same intensities.

One of these optical beams gets transmitted by the beam splitter to the movable mirror whereas; the other gets reflected by the beam splitter to the fixed mirror. Both these beams get reflected back by the respective mirrors and recombine at the beam splitter. This recombined beam coming from the beam splitter then passes through the sample under test. However, the sample absorbs certain amount of energy at each particular wavelength which is then recorded. The detector then detects and measures these absorbed radiations as a function of wavelength (or wavenumber) and lastly transforms the signal mathematically in terms of an IR spectrum also known as *'Absorption Spectrum'* by using Fourier Transformation. But in some cases, the sample transmits certain IR radiations which yields the *'Transmittance Spectrum'* wherein; transmittance (%T) is plotted against wavenumber (cm^{-1}) usually in the range of 4000 cm^{-1} to 400 cm^{-1} [30,31]. In case of 100% transmittance, no absorption of IR radiations occurs. However, if transmittance is 0 % then, all these radiations are said to be absorbed [32].

Both, the absorbance as well as transmittance spectrum can be termed as *'Fingerprint Spectrum'* which is unique for a particular compound as no two different molecular structures can produce the exactly same infrared spectra. The investigation of these IR absorption/transmittance spectra estimates the bonds present in a particular sample (unknown

compound) and determines its structure. Usually, in transmittance spectra, the molecular vibrations appear as dips and as peaks in the absorption spectra.

♣ ***Modes of Vibrations***

When the molecules of a compound or a sample absorb IR radiations, the energy associated with them gets converted into stretching and bending vibrations. In *'Stretching'* modes of vibrations, atoms vibrate linearly in symmetric or asymmetric manner. In this vibration, only the interatomic distance between the two atoms changes continuously. However, the bond angles remain unchanged. The stretching vibrations are further subdivided into symmetric and asymmetric vibrations as demonstrated in Fig. 3.11 (b) [33].

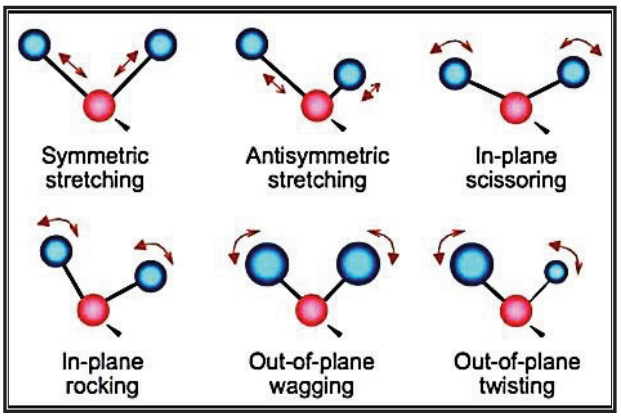

Fig. 3.11 (b) Modes of vibrations: molecular vibrations and rotational modes

❖ **Symmetric Stretching:** When the movement of atoms in a system with respect to particular central atom occurs in the same direction then this type of vibration is known as *'Symmetric Stretching'* vibration.

❖ **Asymmetric Stretching:** In a system if one atom is approaching the central atom but another atom moves away from this central atom, and vice versa then this leads to *'Asymmetric Stretching'* vibration.

Other than the stretching vibrations, the bending vibrations also take place which are further subdivided into scissoring, rocking, wagging and twisting vibrations as illustrated in Fig. 3.11 (b). Various bending vibrations are explained in short as follows [33].

- **Scissoring**: The bond vibration in which two atoms approach each other in the same plane is called '*Scissoring'*. Hence, it is known as *'In-Plane'* scissoring or *'In-Plane'* bending.
- **Rocking**: The movement of atoms in this type of bond vibration takes place in the same direction as well as in the same plane. Thus, this is called *'In-Plane'* rocking or *'In-Plane'* bending.
- **Wagging:** In this type of bond vibration, the two atoms undergo motion up and down the plane with respect to the central atom. This is known as *'Out-of-Plane'* wagging or *'Out-of-Plane'* bending.
- **Twisting:** In this type of bond vibration, one atom moves up the plane with respect to the central atom while the other moves down the plane and vice-versa. This is called *'Out-of-Plane'* twisting or *'Out-of-Plane'* bending.

As the energy required in stretching phenomenon is more than that needed for bending process (general case of a spring), the stretching absorption of bond appears at frequencies higher than that at which the bending absorption of bond appears.

♣ ***Present Study:***

Investigations of structural properties of PVA-PEO blend specimens have been done on the basis of their FT-IR measurements. Further, a small amount of pure constituents and $LiMn_2O_4$ powder is taken individually along with a large amount of KBr in a mortar-pestle, ground gently and thoroughly made into pallets by using *'Hydraulic Press Palletizer'* as shown in Fig. 3.12 (a). FT-IR measurements of these pallets of the respective pure constituents and $LiMn_2O_4$ powder along with those of the films of PVA-PEO blend specimens are carried out by using the *'FT-IR 4100 JASCO Model'* FT-IR instrument as depicted in the Fig. 3.12 (b), in wavenumber ranging from 4000 to 500 cm^{-1} except for $LiMn_2O_4$ powder for which the measurements are carried out in the range of 4000 cm^{-1} to 375 cm^{-1}. This study

further, throws light on crystallinity and/or amorphicity of the pure constituents, polymeric blend specimens and $LiMn_2O_4$ cathode material.

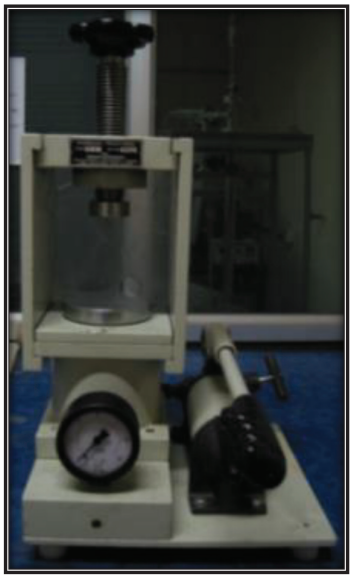

Fig. 3.12 (a) Hydraulic press palletizer

Fig. 3.12 (b) FT-IR 4100 JASCO Model

3.2.4 Scanning Electron Microscopy

'Scanning Electron Microscopy (SEM)' successfully examines various microstructural and morphological features of organic, inorganic, biological, metallic, ceramic, etc. types of samples [11,34-38]. The technique characterizes these materials at a fine scale of micrometre to nanometre owing to high resolution and larger magnification of scanning electron microscopes. As seen from Fig. 3.13, the top of the microscope column consists of electron gun filled with a hairpin filament cathode which produces the illuminating primary monochromatic electron (e^-) beam. This e^- beam thus, released by the cathode is then accelerated by a voltage of 0.5 kV to 30 kV between anode and cathode. But the electrons of the hence, generated e^- beam can disperse or scatter quickly due to their interactions or collisions with other gas molecules or any extraneous particles in the atmosphere. Hence, high

vacuum is applied in the vacuum system in order to prevent so and line up the electrons in the form of a pencil e^- beam.

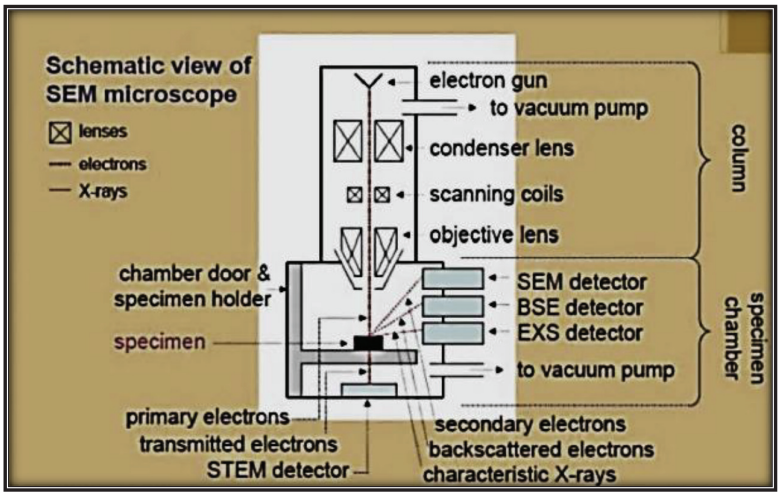

Fig. 3.13 Construction of scanning electron microscope

This e^- beam is later passed through the lens system formed of condenser lens and objective lens. However, the spot size of the generated e^- beam is too large to produce a sharp image. Therefore, in order to adjust/reduce the crossover and the diameter of the e^- beam, the beam is allowed to pass through 1^{st} condenser lens placed below electron gun which condenses the stream of monochromatic electrons as well as limits the amount of current of the beam. This lens basically consists of a condenser aperture which eliminates some high angle electrons and constricts this e^- beam. After passing through 1^{st} condenser lens, the e^- beam passes through the 2^{nd} condenser lens which forms the electrons into a thin, tight and coherent beam and finally focuses it to the scanning coils. As the scanning coils 'sweep' or 'scan' the e^- beam in a grid fashion, this e^- beam dwells on each point for a certain time period as determined by the scanning speed. The e^- beam then passes through the objective lens which successfully de-magnifies its cross-section and focuses it as a probe with a diameter of nanometre scale on the part of the desired sample. This e^- beam then bombards to a small spot of about 50 Å to 100 Å in diameter on the sample's surface. The deflection system moves this e^- beam over the surface of the sample along a line and displaces it finally to a position on the

next line for scanning. In this way, the e^- beam gets sequentially displaced over the entire surface of the sample. But as soon as this primary e^- beam gets incident on the sample, the electrons of the beam, instead of getting penetrated into the sample, get randomly scattered as backscattered electrons (BSE), characteristic X-rays, phonon excitation (heating), Auger electrons, continuum radiations, cathodeluminiscence (CL) and secondary electrons. Each of these scattered electrons or signals thus, produced by the interaction of e^- beam with the sample are finally collected with the sufficient efficiency and detected by the respective detectors. The hence, collected and detected signals by the respective detectors then produce SEM images as displayed on the computer monitor which inform about the morphology and topology of the sample under consideration. The signal generated by the detector system is then processed by the electronic system called *'Signal Processing Unit'* which allows the additional manipulation of the image. The computer hardware disc lastly saves the image in the modern machine which can be viewed as and when required.

♣ ***Present Study***

Fig. 3.14 JEOL JSM-5610LV

Surface morphology of the as prepared PVA-PEO blend specimens of all the series is studied at the constant magnification of 100 X and resolution of 100 μm using *'JEOL JSM-5610LV'* scanning electron microscope as shown in Fig. 3.14.

3.2.5 Ionic Transport Number Measurement

When a salt is mixed with an insulating polymer, the conduction of ion takes place into the polymer matrices. Here, both cations as well as anions have a chance to move into this matrix of polymer electrolyte which leads to the transport of electric charge conduction [39]. Hence, in case of polymer electrolytes, both cations along with anions are expected to be mobile. However, in most of such polymer electrolytes, the free electrons present in the system also contribute in the conduction process. Thus, it is highly essential to understand as to which of the mobile species i.e. ions or electrons provide what fraction of current and conductivity, individually. This can be understood by carrying out *'Transport Number'* measurements of the individual species (ions and electrons). In the polymer electrolytes, as the majority charge carriers are ions which contribute in conductivity, than electrons which negligibly contribute in the conduction process, the *'Ionic Transport Number'* is of a major interest. This ionic transport number is defined as the *'ratio of "conductivity" due to ions to "total (electronic + ionic) conductivity" in a system'* or *'ratio of "current" due to ions to "total (electronic + ionic) current" in a system'*. This ionic transport number can be mathematically written as:

$$t_i = \frac{\sigma_i}{\sigma_t} = \frac{i_i}{i_t} \qquad \ldots\ldots\ldots\ldots\ldots (3.3)$$

where, t_i = ionic transport number, σ_i = conductivity due to ions, σ_t = total (electronic + ionic) conductivity, i_i = current due to ions, i_t = total (electronic + ionic) current. Generally, in case of ideal (pure) ionic electrolytes, $t_i = 1$ and $t_e = 0$ [39]. However, practically, in case of mixed (partially electronic + partially ionic) conducting materials such as polymer electrolytes, the transport number lies between 0 & 1. Hence, for such a case, ionic transport number 't_i' is given as:

$$t_i = \frac{i_t - i_e}{i_t} = \frac{i_t}{i_t} - \frac{i_e}{i_t} = 1 - \frac{i_e}{i_t} = 1 - t_e \qquad \ldots\ldots\ldots\ldots\ldots (3.4)$$

$$\therefore \quad t_i = 1 - t_e \qquad (\text{where, } t_e = \frac{i_e}{i_t}) \qquad \ldots\ldots\ldots\ldots\ldots (3.5)$$

Here, t_e = electronic transport number and i_e = current due to electrons. There are two major methods viz. *'Wagner's Polarization'* and *'dc Polarization'* techniques which measure the ionic transport numbers of various electrolytes including polymer electrolytes. In both these methods, the mixed (ionically + electronically) conducting sample is placed between the two electrodes and this cell is configured as '*Anode*//*Electrolyte*//*Cathode*'.

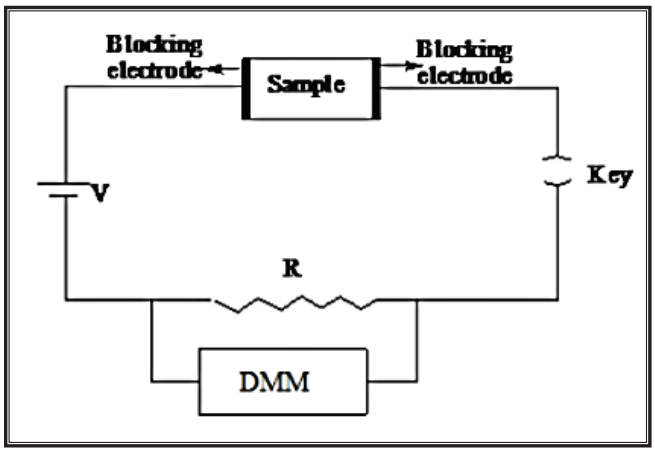

Fig. 3.15 Typical experimental setup for ionic transport number measurement

In Wagner's polarization method, one of the two electrodes sandwiching the electrolytic sample is blocking whereas; the other is non-blocking for mobile charge carriers (ions). Later, a fixed dc potential < decomposition potential of this mixed conducting electrolyte sample under test, is applied across the electrolytic sample configured. The same procedure is followed in dc polarization technique also. However, in this method, both the electrodes sandwiching the electrolytic sample are blocking. Hence, in this case, a uniform dc potential to be applied across the cell assembly should be pretty small. This makes dc polarization technique slightly different from the typical Wagner's polarization method [40-42]. However, in both these techniques, as the dc electric potential is applied across the cell assembly, the current is measured as a function of time using the typical experimental setup for ionic transport number measurement as shown in Fig. 3.15.

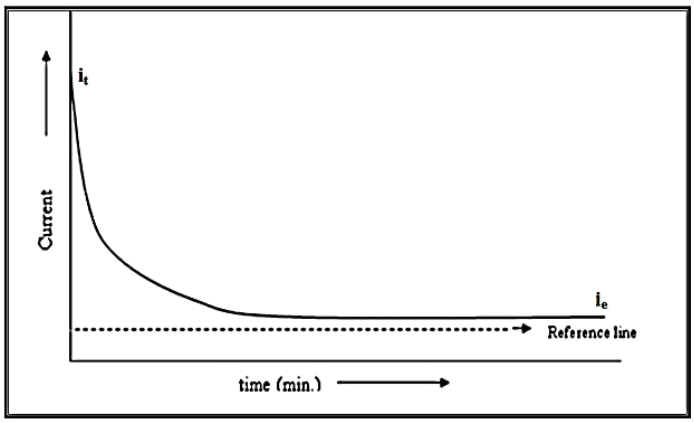

Fig. 3.16 Typical polarization curve

This yields a typical current vs. time plot (polarization curve) as depicted in Fig. 3.16 wherein, both the ionic as well as electronic mobile species contribute to the total (peak) current 'i_t' with a maximum value. This is different from pure ion conductor wherein; peak current or total current 'i_t' is due to ions only as no electrons are available to contribute in the current. However, in mixed ionic conductors such as polymer electrolytes, as the time passes, the applied dc potential across the cell forces more and more ions to move towards the electrodes and to get polarized at electrode-electrolyte interfaces. Such a gradual depletion of ionic species with the passage of time results in the substantial reduction of current from its maximum value as the time increases. After a certain time when all the ions get polarized, current achieves a minimum value and remains low and steady with time. At this stage, as all the ions are completely depleted, the final residual constant current is said to be only due to electrons and hence, termed as *'Electronic Current (i_e)'* [43-45]. Such behaviour of polymer electrolytes is quite different from that of purely ionic conductors wherein; due to the absence of electrons, the final residual current, instead of attaining a constant value, approaches to zero. However, by substituting the values of 'i_e' and 'i_t' in Eq. 3.4, value of ionic transport number 't_i' of a polymer electrolyte can be obtained. By further substituting 't_i' value in Eq. 3.5, the value of electronic transport number 't_e' of this electrolyte can be calculated. In this way, both the Wagner's and dc polarization methods yield ionic as well as electronic transport

numbers of a polymer electrolytic specimen under consideration [43,46-48] and separately provide information regarding the respective ionic and electronic part of conduction.

♣ ***Present Study***

In the present case, polarization study is carried out by using *'dc Polarization Technique'* for which the experimental setup is as depicted in Fig. 3.17. The as prepared PVA-PEO blend specimens of each series are individually sandwiched between a pair of silver (Ag) electrodes and a dc bias of constant voltage (50 mV) is applied across this assembly. As ions in the specimen get polarized at electrode-electrolyte interfaces, the current flowing through the circuit is monitored as a function of time using the '*Keithley 6514 System Electrometer'*. During this process of polarization, the value of initial total current 'i_t', which is due to both electrons and ions (cations + anions), is immediately noted down as soon as the experiment starts up. Expression for this total current in terms of individual currents due to ions and electrons is given as:

$$i_t = i_i + i_e \qquad \ldots\ldots\ldots\ldots\ldots (3.6)$$

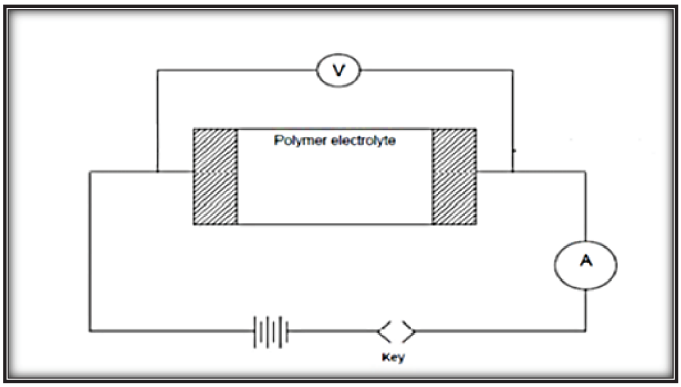

Fig. 3.17 Experimental setup for measuring ionic transport number by dc polarization method

After about 5 to 6 hours all the ions in the specimen get completely polarized and the specimen-based cell delivers the final steady current as *'Electronic Current (i_e)'* which is contributed only due to electrons flowing through the circuit. This electronic current (i_e)

remains low and constant with time. This value of electronic current (i_e) is then noted down, used along with the value of initial total current (i_t) and substituted in the following equation to calculate the value of ionic current (i_i).

$$i_i = i_t - i_e \quad \text{... ... ... (3.7)}$$

In terms of 'i_e' and 'i_t', equation for electronic transport number (t_e) is given as:

$$t_e = \frac{i_e}{i_t} \quad \text{... ... ... (3.8)}$$

Finally, the value of electronic transport number 't_e' obtained from Eq. 3.8 is substituted in the following equation and used to calculate respective value of ionic transport number (t_i).

$$t_i = 1 - t_e \quad \text{... ... ... (3.9)}$$

3.3 Electrical Properties

Suppose a cell assembly consisting of an electronically conducting sample sandwiched between two metallic non-blocking electrodes. If a dc potential is applied across this assembly, the electrical conductivity 'σ' can be measured easily by using two probe or four probe dc methods. However, this dc method is not similarly simple to obtain ionic conductivity when applied to ionic materials wherein; ions are the majority charge carriers.

Basically, in this dc method, current flows only in a single direction which builds up a concentration gradient. Hence, if a dc potential is applied across a cell assembly consisting of an ionically conducting sample, the mobile ions travel rapidly at the respective counter electrodes. But as these ions are unable to travel across the electrode-electrolyte interface they get accumulated at the interface thus, leading to polarization. This phenomenon of polarization of mobile ions occurs quite fast which results in the continuous and rapid increase in the resistance with the passage of time hence, dropping the ionic current. Hence, it is quite tedious to measure the true bulk resistance of an ionically conducting sample viz. polymer electrolyte using this dc method. Such a difficulty can be overcome by considering

an alternative non-destructive ac technique called *'Impedance Spectroscopy'* which is based on the concept of *'Impedance (Z^*)*.

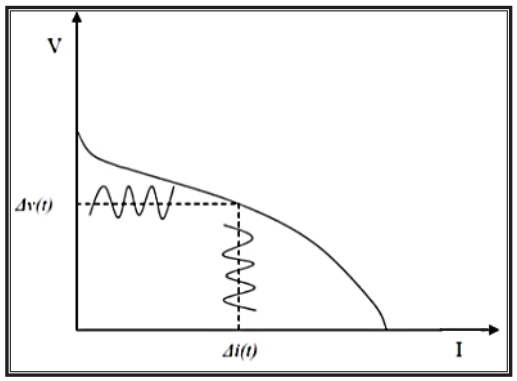

Fig. 3.18 Principle of complex impedance spectroscopy

This method is highly preferred over the dc method as it not only overcomes the limiting properties of dc method but also investigates various electrical processes and dynamic properties of an ion conducting material which further inform about the microscopic nature of the conduction mechanism taking place therein.

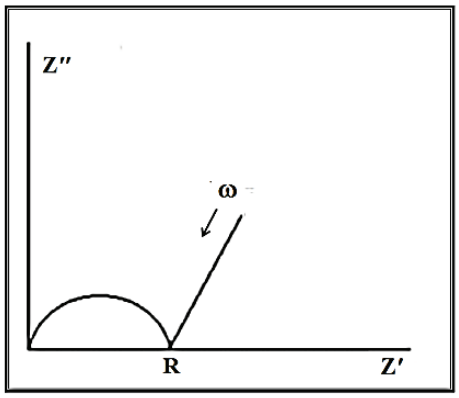

Fig. 3.19 Nyquist Plot of real solid electrolytes

In an impedance spectroscopy experiment, suppose an ion-conducting sample such as a polymer electrolyte is sandwiched between either two blocking or two non-blocking electrodes and let a sinusoidal ac signal of low frequency is applied across this cell assembly under a steady state. Then ac response of this perturbation is measured and determined which may be in the form of voltage or current but different from the applied signal in terms of

phase and amplitude. Such a principle of *'Complex Impedance Spectroscopy'* is diagrammatically shown in Fig. 3.18. Now, there are two parameters by which the voltage and current are related where, the first parameter is Ohm's law defined as *'ratio of voltage maxima to current maxima in time domain when ac signal is applied to a system'* and it is expressed as [49]:

$$\frac{V_{max}}{I_{max}} \quad \ldots\ldots\ldots\ldots\ldots (3.10)$$

The second parameter relating this voltage and current is the phase shift (phase difference) 'θ' between voltage and current. Combination of both these parameters provides the third parameter called 'Magnitude of Impedance ($|Z|$)' of the considered cell assembly. But the impedance (Z^*) is actually complex in nature and can be expressed mathematically as:

$$Z^* = Z' - iZ'' \quad \ldots\ldots\ldots\ldots\ldots (3.11)$$

where, Z' = real part of impedance (= resistance), Z'' = imaginary part of impedance and $i = \sqrt{-1}$. The result of complex impedance measurement of a cell as function of applied signal frequency can be expressed conventionally in a complex plane known as *'Impedance Plot'* or *'Nyquist Plot'* [50-52]. By extrapolating this complex curve to the intercept of real axis (Z'-axis or X-axis), the bulk resistance (R_b) which is actually the dc resistance of the sample, can be determined. By obtaining this bulk resistance (R_b) of the sample under test and by knowing the sample's dimensions (thickness and area), its true bulk (ionic) conductivity can be determined by using the following formula [53].

$$(\sigma) = \left(\frac{1}{R_b}\right) * \left(\frac{l}{A}\right) \quad \ldots\ldots\ldots\ldots\ldots (3.12)$$

The complex conductivity can thus, be obtained in terms of complex impedance as:

$$\sigma^*(\omega) = \left(\frac{l}{A}\right)\left(\frac{Z^*(\omega)}{Z'^2 + Z''^2}\right) = \sigma'(\omega) - i\sigma''(\omega) \quad \ldots\ldots\ldots\ldots\ldots (3.13)$$

where, $i = \sqrt{-1}$, ω = angular frequency = $2\pi f$ (where, f = frequency), l = thickness of the sample, A = cross sectional area of the sample, σ' = real part of conductivity, σ'' = imaginary part of conductivity. Further by using complex impedance (Z^*), complex dielectric permittivity (ε^*) can be obtained as [54]:

$$\varepsilon^*(\omega) = \frac{1}{j\omega C_0 Z^*} = \varepsilon'(\omega) - i\varepsilon''(\omega) \quad \ldots\ldots\ldots\ldots\ldots (3.14)$$

where, C_0 = vacuum capacitance = $\varepsilon_0 \left(\frac{A}{l}\right)$, ε_0 = permittivity of free space = constant, ε' = real part of complex dielectric permittivity also known as *'Dielectric Constant'* and ε'' = imaginary part of complex dielectric permittivity also known as *'Dielectric Loss'*. This complex dielectric analysis informs about the electrode polarization [55]. Next, is the relaxation process occurring in solids which can be understood on the basis of Modulus Formalism [56]. This complex modulus function (M^*) is given in terms of complex impedance (Z^*) as:

$$M^*(\omega) = \frac{1}{\varepsilon^*(\omega)} = j\omega C_0 Z^* = M' + iM'' \quad \ldots\ldots\ldots\ldots\ldots (3.15)$$

where, M' = real part of complex modulus and M'' = imaginary part of complex modulus. The conductivity relaxation effects become prominent in the modulus formalism whereas; the electrode-electrolyte interface polarization effects get supressed here [55]. All these parameters obtained from complex impedance (Z^*) which provide a specific information about the sample upto a certain extent under test, are inter-convertible.

♣ ***Present Study***

For the impedance measurements in the present study, all the PVA-PEO blend specimens serving as electrolytes, are firstly cut into small pieces and then individually kept in between two polished, properly cleaned and spring loaded silver electrodes of the sample holder as shown in Fig. 3.20 (a). The diameter and area of electrodes measured using

micrometre (screw gauge) is 1.798 cm and 2.543 cm^2, respectively. This cell is then kept into a furnace controlled by a mercury contact thermometer and a relay.

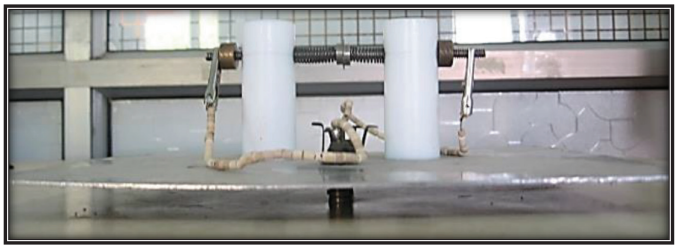

Fig. 3.20 (a) Sample holder

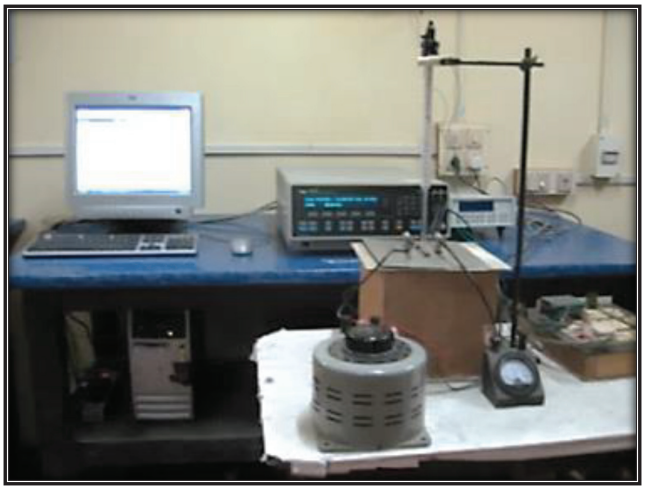

Fig. 3.20 (b) Solartron SI-1260 Impedance Gain/Phase Analyser

These impedance measurements are done using '*Solartron SI-1260 Impedance Gain/Phase Analyser'* as shown in Fig. 3.20 (b) by heating the blend specimens at the interval of 5 °C (or 5 K) in the temperature range of 303 K to 348 K. The frequency of the impedance measurements ranged from 10 Hz to 32 MHz. (However, in some of the studies as provided in the forthcoming chapters, the very high frequency data (> 20 MHz) are omitted (or exempted) due to noise effects).

3.4 Battery Essentials

In the present work, assembly of *'Ag^+ primary polymer battery'* and *'Li^+ primary polymer battery'* is as shown in Fig. 3.21 (a) and Fig. 3.21 (b), respectively. In the preparation of both these Ag^+ and Li^+ primary polymer batteries, the best conducting nano-composite

electrolytes of PPAPA and PPELA series are considered, respectively. Ag^+ primary polymer battery is constructed by employing Ag_2O as cathode and pure silver (Ag) metal as anode. This battery is fabricated with the configuration of Ag //[$PVA_{(50)}$: $PEO_{(50)}$] – 5 wt% $AgNO_3$ – 10 wt% PEG – 6 wt% Al_2O_3 //Ag_2O.

Fig. 3.21 (a) 'Ag^+ primary polymer battery' assembly

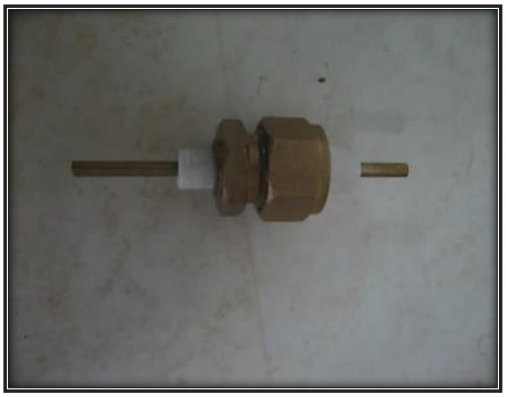

Fig. 3.21 (b) 'Li^+ primary polymer battery' assembly

On the other hand, $LiMn_2O_4$ as cathode and graphite as anode are used in the preparation of Li^+ primary polymer battery which is configured as 'Graphite //[$PVA_{(50)}$: $PEO_{(50)}$] – 6 wt% EC – 9 wt% $LiCF_3SO_3$ – 10 wt% Al_2O_3 //$LiMn_2O_4$'. Both these batteries are thoroughly examined using the setup as depicted in Fig. 3.22.

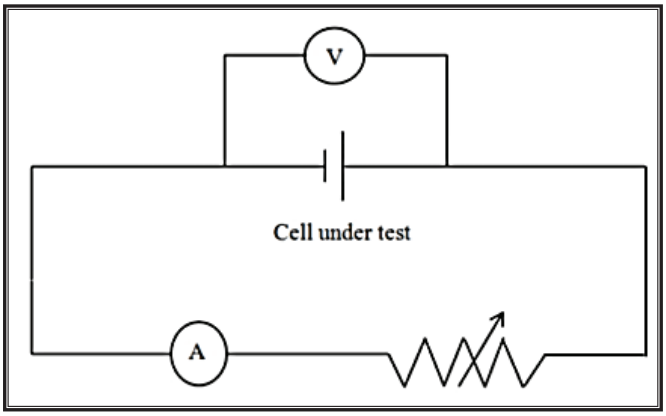

Fig. 3.22 Setup for examining as fabricated Ag^+ & Li^+ primary polymer batteries

Testing of both these Ag^+ as well as Li^+ primary polymer batteries is successfully carried out in open atmosphere at room temperature. The performance of these as prepared batteries

under test can be easily understood on the basis of their respective parameters, usually termed as *'Battery Parameters'*. Hence, some of the essential battery parameters along with the battery components considered in case of the presently prepared batteries are explained briefly as follows [57,58]:

- **Anode**: It is the negative electrode of a cell/battery associated with oxidative chemical reactions which release electrons into the external circuit. Basically, the electrons flow from this negative electrode into the external circuit during discharge of the battery.
- **Cathode**: It is the positive electrode of a cell/battery associated with reductive chemical reactions which gains electrons from the external circuit. Actually, when the battery discharges, the flow of electrons takes place from the external circuit to this positive electrode.
- **Internal Resistance (Impedance)**: Resistance or Impedance which a battery offers to the flow of current.
- **Load**: In case of battery operations the term *'Load'* relates to the energy-consuming device to which electric power is delivered.
- **Open Circuit Voltage (OCV)**: It is the 'constant' potential difference (voltage) between the two electrodes or two terminals (external connections to the battery electrodes) of a battery when no load is applied. This is a condition wherein, no net current flows through the battery circuit. Hence, no net current can be drawn from the battery. In other words, this open circuit voltage (OCV) is actually the voltage developed across battery's terminals when there is no current flow in the external circuit and it is usually near to the thermodynamic voltage of the system.
- **Closed Circuit Voltage (CCV)**: It is the voltage of a battery when the battery produces some current into the external circuit.

- **Terminal Voltage**: It is the potential difference (voltage) between the two electrodes or two terminals (external connections to the battery electrodes) of a battery when a load is applied.
- **Load Voltage**: Voltage of a battery while delivering a current is termed as *'Load Voltage'*. Generally, the voltage of a battery measured upon application of load is lower to that measured in the absence of load (no load or open circuit condition). This phenomenon is likely to occur due to the internal resistance of the battery made up of Ohmic (resistive) losses and polarization losses.
- **Discharge**: A process wherein the battery under test delivers electrical energy to the externally applied load.
- **Capacity**: While going from completely charged state to completely discharged state, a battery is capable of delivering a quantity of stored electrical energy. This capability of the battery to deliver the stored electrical energy is also termed as *'Discharge Capacity'* which is usually measured in terms of ampere-hours (Ah) or milliampere-hours (mAh). However, the amount of charge can be withdrawn from a fully charged battery under the specific conditions only.
- **Specific Capacity**: It is the capacity output of a battery per unit weight usually expressed in terms of Ah kg^{-1} or mAh g^{-1}.
- **Specific Power**: Specific power of a battery can be defined as *'the capacity of a battery to deliver power (power output) per unit weight'*. This parameter is expressed as W kg^{-1} and determines the weight of the battery required to achieve the expected performance target. Likewise specific energy, specific power is also the characteristic of packaging and chemistry of a battery.
- **Specific Energy**: Specific energy, which is usually also termed as *'Gravimetric Energy Density'* is the maximum energy that can be generated (energy output) per unit total mass

of the reactants in a battery. It is also defined as *'the energy output of a battery per unit weight'*. This parameter is expressed as Wh kg^{-1} and determines the weight of the battery required to achieve an expected electric charge and energy consumption of the vehicle in which it is applied. This specific energy is characteristic of packaging and chemistry of a battery.

References

[1] A. Karmakar, A. Ghosh, *Phys. Rev. E* 84 (2011) 051802-1.

[2] R.C. Agrawal, G.P. Pandey, *J. Phys. D: Appl. Phys.* 41 (2008) 223001.

[3] C.W. Nan, L. Fan, Y. Lin, Q. Cai, *Phys. Rev. Lett.* 19 (2003) 266104-1.

[4] A.M. Stephan, *Euro. Poly. J.* 42 (2006) 21.

[5] A.J. Bhattacharyya, T.R. Middya, S. Tarafdar, *Phys. Rev. B* 60 (1999) 909.

[6] P. Bahadur, N.V. Shastry, *Principles of Polymer Science,* second ed., Narosa Publishing House Pvt. Ltd., India, 2005.

[7] K.T. Braam, S. K. Volkman, V. Subramanian, *J. Power Sources* 199 (2012) 367.

[8] X. Zhou, M. Chen, H. Bai, C. Su, L. Feng, J. Guo, *Vacuum* 99 (2014) 49.

[9] A.R. West, *Solid State Chemistry and its Applications,* John Wiley & Sons (Asia) Pte, Ltd., Singapore, 2003.

[10] S.T. Myung, Y. Hitoshi, Y.K. Sun, *Journal of Materials Chemistry* 21 (2011) 9891.

[11] L. Smart, E.A. Moore, *Physical Methods for Characterizing Solids, Solid State Chemistry: An Introduction,* Taylor & Francis, New York, 2005.

[12] U.W. Gedde, *Polymer Physics,* Chapman & Hall, UK, 1995.

[13] W.L. Bragg, *Nature* 90 (1912) 410.

[14] W.L. Bragg, *Proc. Cambridge Philos. Soc.* 17 (1913) 43.

[15] B.D. Cullity, *Elements of X-Ray Diffraction,* Reading, Addison-Wesley Publishing Company, Inc., Massachusetts, 1956.

[16] M.S. Jayswal, *Ph.D. Thesis*, Department of Physics, The M.S. University of Baroda, 2014.

[17] B.E. Warren, *X-ray Diffraction,* Dover Publications, Inc., New York, 1990.

[18] P.F. Fewster, *X-ray Scattering from Semiconductors,* second ed., Imperial College Press, London, 2003.

[19] C. Suryanarayana, M.G. Norton, *X-ray Diffraction: A Practical Approach,* Plenum Press, New York, 1998.

[20] B.D. Cullity, *Elements of X-ray Diffraction,* Addison-Wesley Publishing Company, Inc., second ed., Reading, MA, 1978.

[21] W.W. Wendlandt, *Thermal Methods of Analysis*, second ed., Wiley-Interscience, New York, 1974.

[22] T. Meisel, K. Seybold, *Crit. Rev. Chem.* 12 (1981) 267.

[23] M.P. Sepe, *Thermal Analysis of Polymers*, Rapra Rev. Reports, 8(11) (1997).

[24] L. Reimer, *Scanning Electron Microscopy: Physics of Image Formation and Microanalysis*, Springer, 1998.

[25] V.R. Gowariker, N.V. Viswanathan, J. Sreedhar, *Polymer Science,* New Age International (P) Ltd., Publishers, India, 1986.

[26] L.H. Sperling, *Introduction to Physical Polymer Science*, second ed., John Wiley & Sons, Inc., Singapore, 1993.

[27] C.E. Carraher, Jr., *Introduction to Polymer Chemistry*, second ed., CRC Press Taylor & Francis Group, LLC, USA., 2010.

[28] G.W.H Hohne, W.F. Hemminger, H.J. Flammersheim, *Differential Scanning Calorimetry*, second ed., Springer-Verlag Berlin Heidelberg, New York, 2003.

[29] P. Joge, D.K. Kanchan, P. Sharma, M. Jayswal, D.K. Avasthi, *Radiation Physics and Chemistry* 100 (2014) 74.

[30] H.H. Willard, L.L. Meritt, J.A. Dean, Jr., *Instrumental Methods of Analysis*, Fourth ed., Affiliated East Coast Press Pvt. Ltd., New Delhi, 1965.

[31] G. Chatwal, S. Anand, in: M. Arora, S. Puri (eds.), *Spectroscopy (Atomic and Molecular)*, Himalaya Publishing House, Bombay, 1983, 39.

[32] P.S. Kalsi, *Spectroscopy of Organic Compounds*, sixth ed., New Age International (P) Ltd., Publishers, India, 2004.

[33] S.M. Ashraf, S. Ahmad, U. Riaz, *Experiments in Materials Science and Materials Chemistry-I: A Laboratory Manual of Polymer*s, I.K. International Publishing House Pvt. Ltd., New Delhi, 2009.

[34] A.R. West, *Elements of Solid State Chemistry*, Wiley, New York, 1987.

[35] M von Ardenne, *Zeitschrift fur Physik (in German Language)* 109 (9-10) (1938) 553.

[36] M von Ardenne, *Zeitschrift fur technische Physik (in German Language)* 19 (1938) 407.

[37] C.R. Brundle, C.A. Evans Jr., S. Wilson, *Encyclopaedia of Materials Characterization, Butterworth Heinemann*, a division of Reed Publishing (USA), Inc., USA, 1992.

[38] V.V. Tsukruk, S. Singamaneni, *Scanning Probe Microscopy of Soft Matter: Fundamentals and Practices*, Wiley-VCH Verlag & Co. KGaA, Germany, 2012.

[39] R.C. Agrawal, R.K. Gupta, *J. Mater. Sci.* 34 (1999) 1131.

[40] J.B. Wagner, in: M. Kleitz, J. Dupuy (eds.), *Electrode Processes in Solid State Ionics*, Reidel Publ. Comp., Dordrecht, Holland, 1976, pp. 185.

[41] G.P. Pandey, R.C. Agrawal, S.A. Hashmi, *Journal of Power Sources* 190 (2) (2009) 563.

[42] S.A. Hashmi, S. Chandra, *J. Mater. Sci. Eng. B.* 34 (1995) 18.

[43] J. Schoonman, F.G. Dijkman, *J. Solid State Chem.* 5 (1972) 111.

[44] W.E. Danforth, J.H. Bodine, *J. Franklin Inst.* 260 (1955) 467.

[45] J. Schoonman, A.J.H. Macke, *J. Solid State Chem.* 5 (1972) 105.

[46] C. Wagner, *Z. Elektrochem.* 60 (1956) 4.

[47] A.V. Joshi, J.B. Wagner, *J. Phys. Chem. Solids* 33 (1972) 205.

[48] C. Wagner, *Z. Elektrochem.* 63 (1959) 1027.

[49] J.R. Macdonald, *Impedance Spectroscopy*, John Wiley & Sons, New York, 1987.

[50] I.M. Hodge, M.D. Ingram, A.R. West, *J. Electroanal. Chem.* 74 (1976) 125.

[51] S. Nakamura, H. Nishikawa, T. Aoki, Y. Ogami, *J. Power Sources* 186 (2009) 278.

[52] D.P. Almond, A.R. West, *Solid State Ionics* 11 (1983) 57.

[53] J.R. Macdonald, W.B. Johnson, in: E. Barsoukov, J.R. Macdonald (eds.), *Impedance Spectroscopy Theory, Experiment and Applications*, Wiley-Interscience Press, New York, 2005, pp. 8.

[54] A.K. Jonscher, *Dielectric Relaxation in Solids*, Chalsea Dielectric Press, London, 1983.

[55] A. Bhide, K. Hariharan, *Euro. Poly. J.* 43 (2007) 4253.

[56] P.B. Macedo, C.T. Moynihan, R. Bose, *Phys. Chem. Glass.* 13 (1972) 171.

[57] R.M. Dell, D.A.J. Rand, *Understanding Batteries*, The Royal Society of Chemistry, UK, 2001.

[58] M. Winter, R.J. Brodd, *Chem. Rev.* 104 (2004) 4245.